

pubs.acs.org/JPCL Letter

Efficient DFT Solver for Nanoscale Simulations and Beyond

Xuecheng Shao,* Wenhui Mi,* and Michele Pavanello*



Cite This: J. Phys. Chem. Lett. 2021, 12, 4134–4139



ACCESS

Metrics & More



Supporting Information

ABSTRACT: We present the one-orbital ensemble self-consistent field (OE-SCF), an alternative orbital-free DFT solver that extends the applicability of DFT to beyond nanoscale system sizes, retaining the accuracy required to be predictive. OE-SCF treats the Pauli potential as an external potential updating it iteratively, dramatically outperforming current solvers because only few iterations are needed to reach convergence. OE-SCF enabled us to carry out the largest *ab initio* simulations for silicon-based materials to date by employing only 1 CPU. We computed the energy of bulk-cut Si nanoparticles as a function of their diameter up to 16 nm, and the polarization and interface charge transfer when a Si slab is sandwiched between two metal slabs where lattice matching mandated a large contact area. Additionally, OE-SCF opens the door to adopting even more accurate functionals in orbital-free DFT simulations while still tackling large system sizes.



S ince the mid-1960s, scientists have hoped that one day first-principles device-level and large-scale materials as six and principles device-level and large-scale materials engineering would be feasible and widely available such that computational models could in part or totally replace experiments, reaching a new level of scientific discovery termed Lab-2.0.1 This futuristic vision can be accomplished only if accurate ab initio quantum mechanical electronic structure methods are computationally cheap and can model system sizes beyond the nanoscale. Density functional theory (DFT)^{2,3} is an excellent candidate method as it can be realized in algorithms that scale linearly with system size using either kinetic energy density functionals 4-7 or a combination of appropriate basis sets and approximate eigensolvers.8-11 However, when DFT models nanoscale system sizes, the introduced approximations can limit accuracy. 12,13 The alternative is to require massive computing infrastructures. 14,15 Thus, the promise of reaching Lab-2.0 has so far been unfulfilled. As will become clear below, the proposed one-orbital ensemble self-consistent field (OE-SCF) method brings a fresh perspective to these problems.

To date, there are two kinds of DFT algorithms: Kohn–Sham DFT (KS-DFT) and orbital-free DFT (OF-DFT). KS-DFT is most common and uses a prescription³ whereby the lowest $N_{\rm e}$ eigenvalues (where $N_{\rm e}$ is the number of electrons) of a one-particle Hamiltonian need to be computed. OF-DFT is prescribed to compute just one state, ¹⁶ recovering the effect of the other states with pure density functionals. ¹⁷ Overall, on one hand, KS-DFT is accurate because it computes the non-interacting kinetic energy functional exactly. It is, however, limited in the system sizes it can approach due to the computational complexity required to compute the many eigenstates. ¹⁸ On the other hand, OF-DFT is applicable to large system sizes because the noninteracting kinetic energy is approximated by a pure density functional. However, it is

typically limited in the accuracy it achieves $^{4,5,13,19}_{20,21}$ unless expensive new-generation functionals are employed.

In this work, we propose a new OF-DFT solver, OE-SCF, that is fast, stable, and accurate. Similar to KS-DFT, OE-SCF relies on an iterative solver so that computationally expensive density functionals are seldom evaluated (only once per self-consistent field, SCF, cycle). This allows the employment of a new generation of kinetic energy functionals, retaining accuracy while removing the need to diagonalize bringing down the computational cost considerably compared to either KS-DFT or conventional OF-DFT.

In recent years, a new generation of kinetic energy functionals^{20–22} has enabled OF-DFT to tackle semiconductors^{21,23} and even clusters^{20,22} reproducing KS-DFT within a few hundreds of a meV/atom. Unfortunately, these functionals coupled with conventional OF-DFT solvers require the evaluation of several tens or hundreds of convolution integrals for each energy evaluation, making them computationally expensive.^{21,24–26} Because of this, the new generation of kinetic energy functionals^{20–22} has never been employed in nanoscale simulations.

OE-SCF changes this state of affairs by employing newgeneration kinetic energy functionals at no additional computational cost compared to more approximate functionals. It does so by devising an appropriate SCF procedure. This is a paradigm shift for OF-DFT, as it can now probe system sizes that were

Received: March 4, 2021 Accepted: April 16, 2021 Published: April 22, 2021





unthinkable before with no need to sequester massive computational resources or sacrifice the predictivity of the results. This is precisely the type of development that brings the realization of Lab-2.0 a step closer.

To describe the details of OE-SCF, let us consider the OF-DFT Lagrangian, $\mathcal{L}[n] = E[n] - \mu \Big(\int n(\mathbf{r}) \, \mathrm{d}\mathbf{r} - N_\mathrm{e} \Big)$, which is differentiated to find density functions, $n(\mathbf{r})$, that minimize the total energy, $E[n] = T_\mathrm{s}[n] + E_\mathrm{Hxc}[n] + \int \nu_\mathrm{loc}(\mathbf{r}) \, n(\mathbf{r}) \, \mathrm{d}\mathbf{r} \, (T_\mathrm{s} \, \mathrm{and} \, E_\mathrm{Hxc}$ are the noninteracting kinetic energy and the Hartree exchange-correlation energies and ν_loc is the local external potential), subject to the constraint that the density integrates to a preset number of electrons, N_e . Functional differentiation of the Lagrangian leads to the Euler equation of OF-DFT which can be written in a Schrödinger-like form,

$$\hat{h}_{\rm OF}\phi(\mathbf{r}) = \mu\phi(\mathbf{r}) \tag{1}$$

where we introduced the pseudo wave function $\phi(\mathbf{r}) = \sqrt{n(\mathbf{r})}$, μ is the chemical potential, and the Hamiltonian is given by

$$\hat{h}_{\text{OF}} = -\frac{1}{2}\nabla^2 + \nu_{\text{Hxc}}[n](\mathbf{r}) + \nu_{\text{Pauli}}[n](\mathbf{r}) + \nu_{\text{loc}}(\mathbf{r})$$
(2)

where the Pauli potential is the difference between the total noninteracting kinetic energy potential and the potential of the von Weizsäcker functional, $v_{\text{Pauli}}[n](\mathbf{r}) = v_T[n](\mathbf{r})$ –

$$v_{\text{vW}}[n](\mathbf{r})$$
, where $T_{\text{vW}}[n] = \left\langle \phi \middle| -\frac{1}{2} \nabla^2 \middle| \phi \right\rangle$.

Equation 1 originates from the condition of stationarity of the total energy functional. In KS-DFT, a similar equation is derived to obtain the occupied and virtual KS orbitals.³ Similar to KS-DFT, we expect the direct use of eq 1 in an SCF iterative procedure to pose problems of convergence whenever the Hamiltonian (e.g., in eq 1, the Hamiltonian is the one in eq 2) has a dense spectrum. Since 1969, in KS-DFT this has been resolved by simply employing ensemble densities via smearing of the occupation numbers.²⁷ Because smearing requires the computation of potentially very many states (in a number that grows linearly with system size), if degeneracy had to appear during the self-consistent solution of eq 1, then smearing the occupations would severely deteriorate the OF-DFT's efficiency.

In the OF-DFT literature, ^{17,28,29} eq 1 could not be numerically solved for any system except those of limited size, containing only a few tens of atoms. ^{28–30} We found the issue not to lie in numerical instabilities as previously thought ^{28,29} but instead to be due to the so-called level-swapping problem arising from the degeneracy of frontier states, whereby whenever the energy ordering of occupied and virtual states is swapped from one SCF cycle to the next, the SCF procedure cannot converge. ²⁷ We analyze the degeneracy in the spectrum of the OF-DFT Hamiltonian of eq 2 in Figure 1.

Before introducing our contributions, we should clarify the role of ensemble *N*-representability in OF-DFT simulations. In OF-DFT, by far the most common method for solving for the electronic structure is the direct minimization of the energy functional (DEM hereafter) with respect to the total electron density, namely,

$$n(\mathbf{r}) = \underset{n}{\arg\min} \{ \mathcal{L}[n] \}$$
(3)

which is insensitive to the features of the spectrum of the OF-DFT Hamiltonian in eq 2. In those cases when degenerate or close-to-degenerate levels arise near the frontier orbital (i.e., in

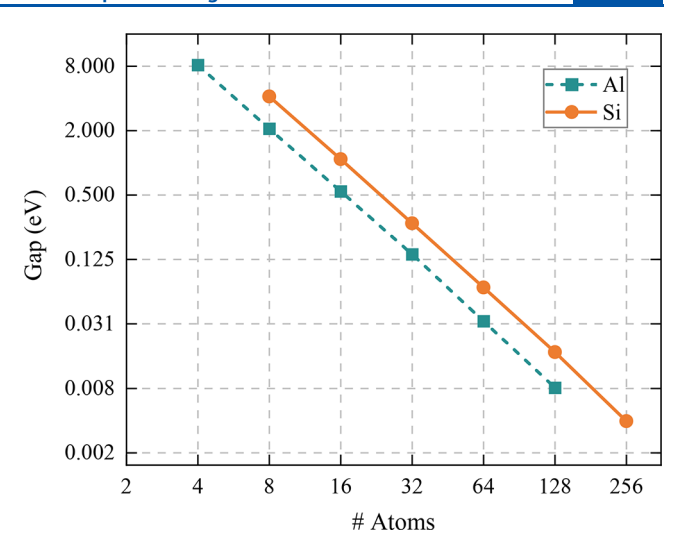


Figure 1. Energy gap between the lowest two energy levels associated with the eigenvalues of the OF-DFT Hamiltonian in eq 2 for supercells of Al and Si bulk systems. The plot is on the log scale, displaying a monotonically decreasing gap with system size. The LMGP kinetic energy functional ²⁰ was used.

OF-DFT, the very first orbital), the density resulting from the minimization of eq 3 will be an ensemble density. Thus, it is clear that in the presence of degeneracy, solving for the OF-DFT problem with eq 1 can be done only by considering ensemble densities, a procedure that, as stated before, cannot be contemplated because it would require computing many solutions of eq 1, defeating the purpose of using OF-DFT as an almost linear-scaling method.

Figure 1 shows the monotonically decreasing gap with increasing system size of bulk Al and Si between the lowest two energy levels of the OF-DFT Hamiltonian of eq 2. This explains why for small model systems (e.g., number of atoms less than 32) this gap is still large enough for the SCF procedure to converge without problems. 28 For large system sizes, this gap is too small, and the level-swapping problem appears to impede the SCF convergence of the OF-DFT problem. As mentioned, a typical way around this is to access ensemble N-representable densities by slightly smearing the occupations across states within a small window of energy that is still big enough not to fluctuate too much from one SCF cycle to the next.²⁷ Once again, this may appear not to be an option for OF-DFT because smearing would require computing by diagonalization a number of states that grows linearly with system size, thereby defeating the purpose of using OF-DFT (i.e., to avoid the $O(N^3)$ complexity of diagonalizations).

OE-SCF solves the problem by introducing ensemble densities and including the Pauli potential in an iterative fashion. OE-SCF's computational protocol is as follows:

- 1. Given a guess density at iteration i, $n_i(\mathbf{r})$ computes the Pauli potential, $\nu_{\text{Pauli}}[n_i](\mathbf{r})$.
- 2. An auxiliary energy functional and the associated Lagrangian are defined, namely,

$$\mathcal{L}_{\text{OE-SCF}}[n, n_i] = T_{\text{vW}}[n] + E_{\text{Hxc}}[n] + \int [v_{\text{loc}}(\mathbf{r}) + v_{\text{Pauli}}[n_i](\mathbf{r})]n(\mathbf{r}) d\mathbf{r}$$
(4)

3. $\mathcal{L}_{\text{OE-SCF}}$ is minimized with respect to variations in $n(\mathbf{r})$, namely,

Table 1. Comparing OE-SCF with Other OF-DFT Solvers^a

method	functional to minimize	external potential $(u_{ m ext})$	ensemble	SCF
DEM	$T_{\text{vW}}[n] + E_{\text{Hxc}}[n] + T_{\text{Pauli}}[n] + \int v_{\text{ext}}(\mathbf{r}) \ n(\mathbf{r}) \ d\mathbf{r}$	$ u_{ m loc}({f r})$	yes	no
SCF	$T_{\text{vW}}[n] + \int \nu_{\text{ext}}(\mathbf{r}) \ n(\mathbf{r}) \ d\mathbf{r}$	$v_{\text{Hxc}}[n_i](\mathbf{r}) + v_{\text{Pauli}}[n_i](\mathbf{r}) + v_{\text{loc}}(\mathbf{r})$	no	yes
OE-SCF	$T_{\text{vW}}[n] + E_{\text{Hxc}}[n] + \int v_{\text{ext}}(\mathbf{r}) \ n(\mathbf{r}) \ d\mathbf{r}$	$v_{\text{Pauli}}[n_i](\mathbf{r}) + v_{\text{loc}}(\mathbf{r})$	yes	yes

^aThe external potential at iteration *i* is to be considered constant during energy minimization. After the minimization is completed, the density-dependent parts of the external potential are updated, as is done in typical SCF procedures. The acronyms are as follows: DEM, direct energy minimization; SCF, self-consistent field; and OE-SCF, the newly proposed DFT solver. OE-SCF probes assemble *N*-representable densities without the need to compute extra eigenstates through diagonalization.

$$n_{i+1} = \underset{n}{\arg\min} \{ \mathcal{L}_{\text{OE-SCF}}[n, n_i] \}$$
 (5)

which, following the reasoning reported after eq 3, will yield an ensemble density whenever the underlying Hamiltonian features (quasi)degeneracy. For clarity, the underlying Hamiltonian in this case is

$$\hat{h}_{\rm OF} = -\frac{1}{2} \nabla^2 + \nu_{\rm Hxc}[n](\mathbf{r}) + \underbrace{\nu_{\rm Pauli}[n_i](\mathbf{r}) + \nu_{\rm loc}(\mathbf{r})}_{\text{external potential at iteration } i}$$
 (6)

4. Steps 1-3 are repeated until convergence is achieved (e.g., $|E[n_i] - E[n_{i+1}]| < 10^{-6}$ Hartree for three consecutive cycles).

As indicated in eq 6 as well as in Table 1, in OE-SCF the external potential includes the local (pseudo)potential and the Pauli potential (at iteration *i*) which contains the most expensive energy term in OF-DFT when new-generation kinetic energy functionals are employed (i.e., the nonlocal part). In this way, OE-SCF needs to evaluate the Pauli potential only once for each SCF cycle. A strong motivation for our work is given by a similar procedure, ³⁰ which was shown to be successful for bulk systems when the WGC functional ³¹ is employed.

Before presenting results from OE-SCF, let us enumerate the computational details. All OF-DFT computations presented in this work are carried out with DFTpy.²⁶ A kinetic energy cutoff of 600 eV is employed in all OF-DFT calculations except for interfaces and surfaces, where we used a larger cutoff of 1200 eV. We adopt the following exchange-correlation functionals: local density approximation (LDA)³² for all bulks, clusters, and surface energies and revised Perdew-Burke-Ernzerhof (revPBE)³³ for interfaces. Reference KS-DFT results are calculated with the same pseudopotentials as used for OF-DFT (i.e., local pseudopotentials (LPPs), 34,35 see the Supporting Information for additional details) as well as nonlocal ultrasoft pseudopotentials (USPP).36 The calculations with USPPs are carried out with Quantum-ESPRESSO (QE)³⁷ with a 70 Ry kinetic energy cutoff for the wave functions. The KS-DFT calculations with LPPs are performed by CASTEP³⁸ with a 1000 eV cutoff, ensuring that the total energies converge within 1 meV/atom. We adopt the truncated Newton method for the direct energy minimization (DEM) algorithm used to minimize $\mathcal{L}[n]$ and $\mathcal{L}_{\text{OE-SCF}}[n, n_i]$. The details of this method can be found in section 2.3 of ref 25.

In Table 2, we show that the number of Pauli potential calls for the commonly adopted DEM method grows with system size, while for OE-SCF, the number of potential calls is much reduced and is also insensitive to system size. In OE-SCF, the von Weizsäcker and the Hartree exchange-correlation potentials are invoked as often as in the DEM method. However, they are computationally affordable if (semi)local xc functionals are adopted (as is most often the case).

Table 2. Total Number of Pauli Potentials and Energy Calls during a Single-Point Calculation for Bulk Aluminum and Silicon a

	aluminum		silicon		
no. of atoms	DEM	OE-SCF	DEM	OE-SCF	
8	41	10	67	20	
32	41	10	67	20	
128	59	13	92	13	
512	200	12	211	13	
2048	595	8	531	10	

^aFor OE-SCF, the number of calls is equal to the number of SCF cycles needed to reach self-consistency. The LMGP nonlocal kinetic energy functional was employed.

We have studied ways in which density mixing can be used to accelerate the convergence of OE-SCF. We have implemented a density mixing method analogous to Pulay's DIIS. ³⁹ However, for the systems considered in this work, we notice only a small improvement when density mixing is included, so we decided not to feature results from density-mixing-aided OE-SCF. It is possible that the need for mixing is system-dependent. Thus, we will keep density mixing in OE-SCF's implementation in the DFTpy software. ²⁶

The number of FFT calls for OE-SCF follows the same trend as for the potential calls, i.e., it is almost constant for varying system sizes as shown in Tables S1 and S2. From the timings reported in Figure 2, it is clear that OE-SCF is superior to DEM, cutting the timing down by orders of magnitude in comparison to the current state of the art, maintaining linear scalability with system sizes.

OE-SCF reproduces the excellent results of new-generation kinetic energy functionals previously obtained by DEM for

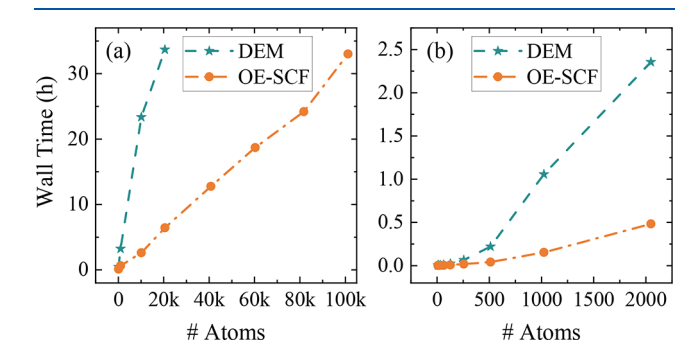


Figure 2. Wall times for a single-point calculation of (a) Si clusters and (b) Si bulk supercells. DEM is the commonly adopted direct energy minimization method in OF-DFT simulations. OE-SCF is the newly proposed DFT solver. Timings for Al clusters and bulk supercells are available in the Supporting Information.⁴⁰ The LMGP kinetic energy functional²⁰ was used.

clusters and bulk semiconductors, ^{20,21} indicating that despite the iterative nature, it reaches the variational minimum of the energy functional. In Figure 3, we compare OE-SCF total

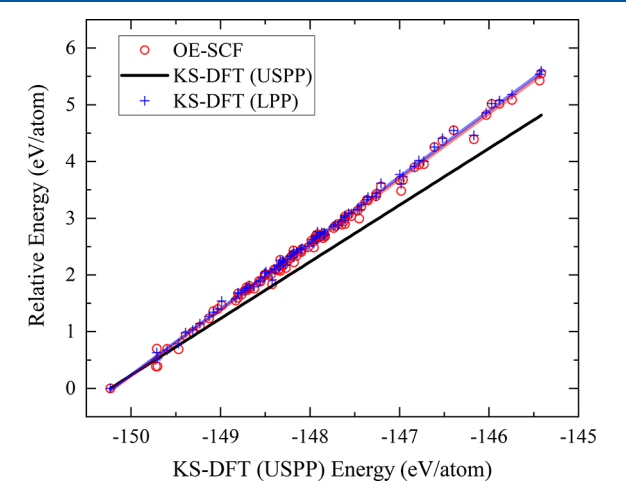


Figure 3. Total energies of 100 random structures of Si_{200} clusters obtained by OE-SCF in comparison with the reference KS-DFT results with either USPPs³⁶ or LPPs.³⁴ The latter pseudopotentials are also employed in OE-SCF.

energies (which in this work are always computed with the LMGP nonlocal kinetic energy functional) against KS-DFT for 100 random structures of 200-atom silicon clusters. The random Si cluster structures are generated by CALYPSO $^{41-43}$ with the restriction that the minimum interatomic distance is 2.2 Å 20 and its nearest-neighboring periodic images are more than 12 Å apart to ensure the creation of physically feasible structures.

As expected, Figure 3 and Table S4 show that OE-SCF's energies lie essentially on top of KS-DFT with LPP pseudopotentials and very close to KS-DFT with USPP pseudopotentials. To better understand how well OE-SCF ranks the 100 random Si cluster structures, we report in Table S4 the ranking residual standard error (RSE). This is a measure of the error from the trendlines plotted in Figure 3 (i.e., deviation from the perfect ranking score). We find that OE-SCF's RSE is 95/75/66 meV for $Si_{100/200/300}$. We remark that the slopes of the ranking trend line for KS-DFT (LPP) are exactly the same as OE-SCF, and its RSE is 68/54/54 meV. This shows that the majority of OE-SCF's RSE value is not due to the kinetic energy functional employed but rather due to the inherent differences between LPPs and USPPs. To further quantify the predictivity and accuracy of our approach, we computed surface energies for Si, Mg, and Al and compared them against those measured by various experiments. As shown in Table S5, OE-SCF reproduces the experimental results semiquantitatively in line with the expected accuracy of a DFT method.

To showcase the ability of OE-SCF to approach nanoscale systems, we compute the electronic structure of bare and hydrogen-passivated Si nanoparticles (Si-NPs) of several sizes (up to 102 501 Si atoms) and a polyhedral shape. The atomic coordinates of these Si-NPs can be found in the Supporting Information. Figure 4 also showcases a plot of the Si-NP's total energy per Si atom converging to the Si bulk value according to a power law. This reproduces previous studies 44,45 up to 7 nm and extends them all the way up to convergence. With OE-SCF, not only is it possible to verify the correctness of the empirical power law but we also do so by employing a single CPU! In Figure S3,

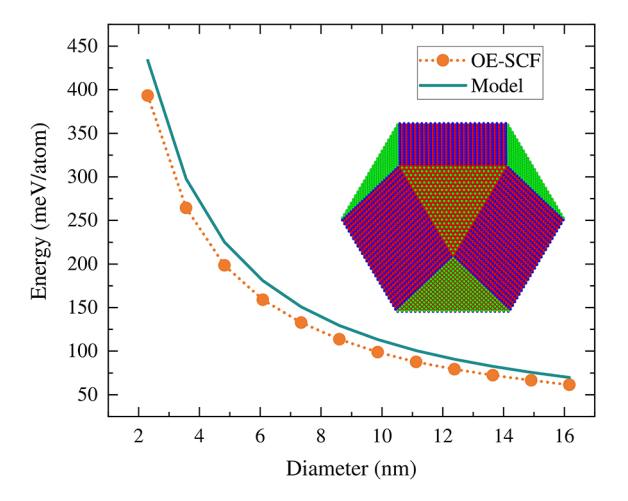


Figure 4. Total energy per Si atom versus nanoparticle diameter (dashed orange curve with circles, OE-SCF; solid green curve, empirical formula taken from ref 44). The inset shows the largest Si nanoparticle considered containing 102 501 Si atoms.

we also show that the energy needed to passivate the Si-NPs used in the study of Figure 4 also decays according to a similar power law. This indicates that the decay law should also apply to hydrogen-passivated Si-NPs and not only to bare Si-NPs.

As a second example, we inspect the electronic structure of interfaces between unreconstructed bare and hydrogen-passivated Si(111) surfaces and Al and Mg metals. We wish to highlight the usefulness of OE-SCF when interfaces are considered. It is often difficult to use DFT methods to describe interfaces because the crystal pacing of one surface rarely matches that of another surface. With that, large slab sizes, most times outside DFT's realm of applicability, need to be considered to avoid introducing artificial strain into the system.

Figure 5a shows the interface considered consisting of six layers of the Si(111) surface passivated by hydrogen atoms (the

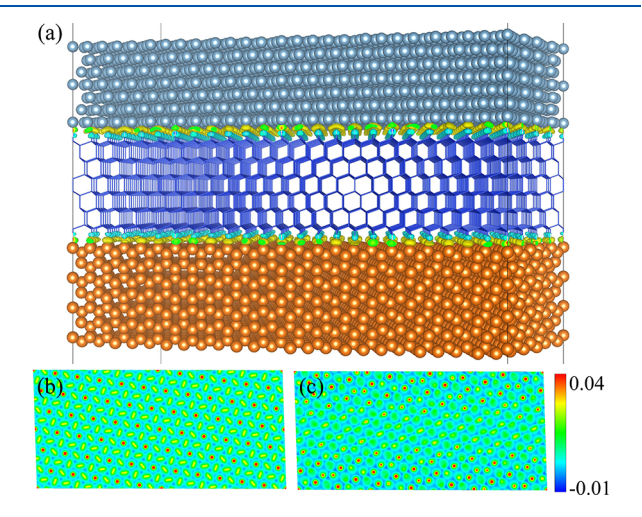


Figure 5. Si-metal interfaces. (a) Al(111) (top), Si(111) (middle), and Mg(100) (bottom, see also Figures S4 and S5 for other configurations) which also feature the isosurface plot of the polarization density, $n_{\rm pol}({\bf r})$, defined by subtracting the electron densities of the isolated Mg, Si, and Al slabs from the total electron density of the system for Si–Al and Si–Mg, respectively. (b, c) Interface plane cuts depicting isovalues of the polarization density. (b) Perfectly symmetrical interface polarization density. (c) Lattices of Mg(100) and Si(111) differ.

of Al(111) on top and seven layers of Mg(100) at the bottom. (The interface with Mg(001) is available in Figure S5.) The figure also shows the interface polarization density, n_{pol} (i.e., the charge density difference between the formed interface and the isolated slabs). As we can see from Figure 5a and more clearly in the interface plane cuts in Figure 5b,c, the interface polarization density results in the buildup of electrons at the interface. This is consistent with the physics of semiconductor interfaces⁴⁷ and the formation of interface electron gases. 48 We went further and computed the charge of the interface by simply computing the integral $C_i = \frac{1}{2A} \int_{I_i} |n_{\text{pol}}(\mathbf{r})| \, d\mathbf{r}$, where $n_{\text{pol}} = n - n_{\text{Al}} - n_{\text{Mg}} - n_{\text{Si}}$, Ais the surface area, and the integration domains, I_{ν} include either of the interfaces. The values are $C_{\text{SiMg}} = 1.04(1.10) \text{ eÅ}^{-2}$ and $C_{\text{SiAl}} = 1.14(1.40) \text{ eÅ}^{-2}$ (unpassivated Si interfaces are in parentheses), showing the slight increase in induced polarization when Si has dangling bonds compared to the hydrogenpassivated surface. Even though a similar increase is expected as is known for other types of interfaces, ⁴⁸ we will further analyze

this system, including better sampling of the nuclear

configurations in follow-up simulations.

bare Si(111) surface is available in Figure S4) with seven layers

In conclusion, we developed a new DFT solver, called OE-SCF, that leverages recent advances in OF-DFT development to output a computationally cheap and accurate ab initio electronic structure method. The key aspect of OE-SCF is its ability to still make use of an SCF-like solver capable of sampling ensemble Nrepresentable electron densities while avoiding the diagonalization of the Hamiltonian. We showcase OE-SCF's computational linear scalability with system sizes well into the hundreds of thousands of atoms for clusters and bulk systems employing merely a single CPU. Finally, OE-SCF's predictivity is tested by computing for the first time with an ab initio method the energy decay law with Si nanoparticles having realistic sizes (of up to 16 nm in diameter). We also confirm the decay law which to date had been tested only with ab initio methods for nanoparticles of up to 7 nm in size. Additionally, we showcase examples of Simetal interfaces where matching crystal pacing is often a showstopper due to the large simulation cells needed to represent the inherent periodicity of the interface. We compute the interfaceinduced polarization and interfacial charge transfer predicting slightly larger charge transfer for the interfaces with the unpassivated Si surface.

We have provided important preliminary results indicating that the proposed OE-SCF method will replace the universally adopted DEM method as the solver of choice in orbital-free DFT software due to its superior stability and computational time to solution. Simultaneously, because OE-SCF needs to evaluate complex functionals only a dozen times regardless of the system size, it will enable the formulation and deployment of even more complex density functionals than currently available for use in predictive beyond-nanoscale DFT simulations.

ASSOCIATED CONTENT

Supporting Information

The Supporting Information is available free of charge at https://pubs.acs.org/doi/10.1021/acs.jpclett.1c00716.

Additional computational details; structures; and supplementary figures and tables (PDF)

AUTHOR INFORMATION

Corresponding Authors

Xuecheng Shao — Department of Chemistry, Rutgers University, Newark, New Jersey 07102, United States; Email: xuecheng.shao@rutgers.edu

Wenhui Mi — Department of Chemistry, Rutgers University, Newark, New Jersey 07102, United States; ⊙ orcid.org/ 0000-0002-1612-5292; Email: wenhui.mi@rutgers.edu

Michele Pavanello — Department of Chemistry and Department of Physics, Rutgers University, Newark, New Jersey 07102, United States; orcid.org/0000-0001-8294-7481; Email: m.pavanello@rutgers.edu

Complete contact information is available at: https://pubs.acs.org/10.1021/acs.jpclett.1c00716

Notes

The authors declare no competing financial interest.

ACKNOWLEDGMENTS

This material is based upon work supported by the National Science Foundation under grants nos. CHE-1553993 and OAC-1931473. We thank the Office of Advanced Research Computing at Rutgers for providing access to the Amarel cluster. X.S. acknowledges the Molecular Sciences Software Institute for support through a Software Investment Fellowship.

REFERENCES

- (1) Gould, T. Welcome to Lab 2.0 where computers replace experimental science.; https://theconversation.com/welcome-to-lab-2-0-where-computers-replace-experimental-science-57271, The Conversation, 2016
- (2) Hohenberg, P.; Kohn, W. Inhomogeneous Electron Gas. Phys. Rev. 1964, 136, B864.
- (3) Kohn, W.; Sham, L. J. Self-Consistent Equations Including Exchange and Correlation Effects. *Phys. Rev.* **1965**, *140*, A1133.
- (4) Wang, Y. A.; Carter, E. A. In *Theoretical Methods in Condensed Phase Chemistry*; Schwartz, S. D., Ed.; Kluwer: Dordrecht, 2000; pp 117–184
- (5) Witt, W. C.; Beatriz, G.; Dieterich, J. M.; Carter, E. A. Orbital-free density functional theory for materials research. *J. Mater. Res.* **2018**, *33*, 777–795.
- (6) Shao, X.; Xu, Q.; Wang, S.; Lv, J.; Wang, Y.; Ma, Y. Large-scale ab initio simulations for periodic system. *Comput. Phys. Commun.* **2018**, 233. 78–83.
- (7) Hung, L.; Carter, E. A. Accurate simulations of metals at the mesoscale: Explicit treatment of 1 million atoms with quantum mechanics. *Chem. Phys. Lett.* **2009**, 475, 163–170.
- (8) Goedecker, S. Linear scaling electronic structure methods. *Rev. Mod. Phys.* **1999**, *71*, 1085.
- (9) Bowler, D. R.; Miyazaki, T. O(N) Methods in Electronic Structure Calculations. *Rep. Prog. Phys.* **2012**, *75*, 036503.
- (10) Liou, K.-H.; Yang, C.; Chelikowsky, J. R. Scalable implementation of polynomial filtering for density functional theory calculation in PARSEC. *Comput. Phys. Commun.* **2020**, 254, 107330.
- (11) Sena, A. M. P.; Miyazaki, T.; Bowler, D. R. Linear Scaling Constrained Density Functional Theory in CONQUEST. *J. Chem. Theory Comput.* **2011**, *7*, 884–889.
- (12) González, D. J.; González, L. E.; López, J. M.; Stott, M. J. Dynamical properties of liquid Al near melting: An orbital-free molecular dynamics study. *Phys. Rev. B: Condens. Matter Mater. Phys.* **2002**, *65*, 184201.
- (13) Wang, L.-W.; Teter, M. P. Kinetic-energy functional of the electron density. *Phys. Rev. B: Condens. Matter Mater. Phys.* **1992**, 45, 13196–13220.

- (14) Wesolowski, T. A.; Shedge, S.; Zhou, X. Frozen-Density Embedding Strategy for Multilevel Simulations of Electronic Structure. *Chem. Rev.* **2015**, *115*, 5891–5928.
- (15) Nakata, A.; Baker, J. S.; Mujahed, S. Y.; Poulton, J. T. L.; Arapan, S.; Lin, J.; Raza, Z.; Yadav, S.; Truflandier, L.; Miyazaki, T.; et al. Large scale and linear scaling DFT with the CONQUEST code. *J. Chem. Phys.* **2020**, *152*, 164112.
- (16) Fermi, E. Un Metodo Statistico per la Determinazione di alcune Prioprietà dell'Atomo. *Rend. Accad. Naz. Lincei* **1927**, *6*, 602–607.
- (17) Karasiev, V. V.; Trickey, S. B. Issues and challenges in orbital-free density functional calculations. *Comput. Phys. Commun.* **2012**, *183*, 2519–2527.
- (18) Moussa, J. E.; Baczewski, A. D. Assessment of localized and randomized algorithms for electronic structure. *Electron. Struct.* **2019**, *1*, 033001
- (19) Wang, Y. A.; Govind, N.; Carter, E. A. Orbital-free kinetic-energy density functionals with a density-dependent kernel. *Phys. Rev. B: Condens. Matter Mater. Phys.* **1999**, *60*, 16350–16358.
- (20) Mi, W.; Pavanello, M. Orbital-Free DFT Correctly Models Quantum Dots When Asymptotics, Nonlocality and Nonhomogeneity Are Accounted For. *Phys. Rev. B: Condens. Matter Mater. Phys.* **2019**, 100, 041105.
- (21) Huang, C.; Carter, E. A. Nonlocal orbital-free kinetic energy density functional for semiconductors. *Phys. Rev. B: Condens. Matter Mater. Phys.* **2010**, *81*, 045206.
- (22) Xu, Q.; Lv, J.; Wang, Y.; Ma, Y. Nonlocal kinetic energy density functionals for isolated systems obtained via local density approximation kernels. *Phys. Rev. B: Condens. Matter Mater. Phys.* **2020**, *101*, 045110.
- (23) Mi, W.; Genova, A.; Pavanello, M. Nonlocal kinetic energy functionals by functional integration. *J. Chem. Phys.* **2018**, *148*, 184107.
- (24) Chen, M.; Xia, J.; Huang, C.; Dieterich, J. M.; Hung, L.; Shin, I.; Carter, E. A. Introducing PROFESS 3.0: An advanced program for orbital-free density functional theory molecular dynamics simulations. *Comput. Phys. Commun.* **2015**, *190*, 228–230.
- (25) Mi, W.; Shao, X.; Su, C.; Zhou, Y.; Zhang, S.; Li, Q.; Wang, H.; Zhang, L.; Miao, M.; Wang, Y.; et al. ATLAS: A real-space finite-difference implementation of orbital-free density functional theory. *Comput. Phys. Commun.* **2016**, 200, 87–95.
- (26) Shao, X.; Jiang, K.; Mi, W.; Genova, A.; Pavanello, M. DFTpy: An efficient and object-oriented platform for orbital-free DFT simulations. *Wiley Interdiscip. Rev.: Comput. Mol. Sci.* **2021**, *11*, No. e1482.
- (27) Slater, J. C.; Mann, J. B.; Wilson, T. M.; Wood, J. H. Nonintegral Occupation Numbers in Transition Atoms in Crystals. *Phys. Rev.* **1969**, 184, 672–694.
- (28) Lehtomäki, J.; Makkonen, I.; Caro, M. A.; Harju, A.; Lopez-Acevedo, O. Orbital-free density functional theory implementation with the projector augmented-wave method. *J. Chem. Phys.* **2014**, *141*, 234102.
- (29) Espinosa Leal, L. A.; Karpenko, A.; Caro, M. A.; Lopez-Acevedo, O. Optimizing a parametrized Thomas-Fermi-Dirac-Weizsäcker density functional for atoms. *Phys. Chem. Chem. Phys.* **2015**, *17*, 31463–31471.
- (30) Ghosh, S.; Suryanarayana, P. Higher-order finite-difference formulation of periodic Orbital-free Density Functional Theory. *J. Comput. Phys.* **2016**, 307, 634–652.
- (31) Wang, Y. A.; Govind, N.; Carter, E. A. Orbital-free kinetic-energy density functionals with a density-dependent kernel. *Phys. Rev. B: Condens. Matter Mater. Phys.* **1999**, *60*, 16350.
- (32) Perdew, J. P.; Zungér, A. Self-Interaction Correction To Density-Functional Approximations For Many-Electron Systems. *Phys. Rev. B: Condens. Matter Mater. Phys.* **1981**, 23, 5048.
- (33) Zhang, Y.; Yang, W. Comment on "Generalized Gradient Approximation Made Simple. *Phys. Rev. Lett.* **1998**, *80*, 890.
- (34) Huang, C.; Carter, E. A. Transferable local pseudopotentials for magnesium, aluminum and silicon. *Phys. Chem. Chem. Phys.* **2008**, *10*, 7109.

- (35) Mi, W.; Zhang, S.; Wang, Y.; Ma, Y.; Miao, M. First-principle optimal local pseudopotentials construction via optimized effective potential method. *J. Chem. Phys.* **2016**, *144*, 134108.
- (36) Dal Corso, A. Pseudopotentials periodic table: From H to Pu. Comput. Mater. Sci. **2014**, *95*, 337–350.
- (37) Giannozzi, P.; Baroni, S.; Bonini, N.; Calandra, M.; Car, R.; Cavazzoni, C.; Ceresoli, D.; Chiarotti, G. L.; Cococcioni, M.; Dabo, I.; et al. QUANTUM ESPRESSO: a modular and open-source software project for quantum simulations of materials. *J. Phys.: Condens. Matter* **2009**, *21*, 395502.
- (38) Clark, S. J.; Segall, M. D.; Pickard, C. J.; Hasnip, P. J.; Probert, M. J.; Refson, K.; Payne, M. First principles methods using CASTEP. *Z. Kristallogr. Cryst. Mater.* **2005**, 220, 567–570.
- (39) Pulay, P. Convergence Acceleration of Iterative Sequences. The Case of SCF Iteration. *Chem. Phys. Lett.* **1980**, *73*, 393–398.
- (40) See the Supporting Information for additional tables and figures.
- (41) Wang, Y.; Lv, J.; Zhu, L.; Ma, Y. CALYPSO: A method for crystal structure prediction. *Comput. Phys. Commun.* **2012**, *183*, 2063–2070.
- (42) Wang, Y.; Lv, J.; Zhu, L.; Ma, Y. Crystal structure prediction via particle-swarm optimization. *Phys. Rev. B: Condens. Matter Mater. Phys.* **2010**, 82, 094116.
- (43) Lv, J.; Wang, Y.; Zhu, L.; Ma, Y. Particle-swarm structure prediction on clusters. J. Chem. Phys. 2012, 137, 084104.
- (44) Zhao, Y.; Kim, Y.-H.; Du, M.-H.; Zhang, S. First-Principles Prediction of Icosahedral Quantum Dots for Tetravalent Semi-conductors. *Phys. Rev. Lett.* **2004**, 93, 015502.
- (45) Zhou, Y.; Saad, Y.; Tiago, M. L.; Chelikowsky, J. R. Parallel self-consistent-field calculations via Chebyshev-filtered subspace acceleration. *Phys. Rev. E* **2006**, *74*, 066704.
- (46) Farmanbar, M.; Brocks, G. First-principles study of van der Waals interactions and lattice mismatch atMoS2/metalinterfaces. *Phys. Rev. B: Condens. Matter Mater. Phys.* **2016**, 93, 085304.
- (47) Franciosi, A. Heterojunction band offset engineering. *Surf. Sci. Rep.* **1996**, *25*, 1–140.
- (48) Rotenberg, E.; Koh, H.; Rossnagel, K.; Yeom, H.; Schäfer, J.; Krenzer, B.; Rocha, M.; Kevan, S. Indium 7×3 on Si (111): a nearly free electron metal in two dimensions. *Phys. Rev. Lett.* **2003**, *91*, 246404.